RSC Advances

PAPER

View Article Online
View Journal | View Issue

Cite this: *RSC Adv.*, 2020, **10**, 5294

Folic acid modified Fe_3O_4 nanoclusters by a one-step ultrasonic technique for drug delivery and MR imaging†

Meng-Yu Fei,‡[a] Meng-Meng Song,‡[bc] Pei Wang,[bc] Gao-zong Pang,[bc] Jing Chen,[b] Da-Peng Lu,[d] Rui Liu,[b] Gui-Yang Zhang,[b] Ting-Ting Zhao,[b] Yu-Xian Shen *[bc] and Yong-Qiang Yu*[a]

Received 19th November 2019
Accepted 17th January 2020

DOI: 10.1039/c9ra09670a

rsc.li/rsc-advances

Multifunctional nanoclusters based on Fe_3O_4 nanoparticles for magnetic resonance imaging (MRI) and drug delivery are reported here. At first, oleic acid (OA)-coated Fe_3O_4 nanoparticles were prepared. Then block copolymer Pluronic F127 or folic acid (FA) conjugated-Pluronic F127 was used to modify the hydrophobic nanoparticles to become hydrophilic Fe_3O_4@F127 nanoclusters *via* facile ultrasonic treatment. During this process, drug molecules can also be introduced into the nanoclusters and therefore the targeted drug delivery system was formed. Next, we verified the feasibility of the nanoclusters as drug delivery vehicles and magnetic contrast agents. The nanoclusters have an average size of 200 nm and remained stable in water for long periods. Folic acid-modified nanoclusters showed an enhanced intracellular uptake into HepG2 cells by using both cellular iron amount analysis and flow cytometry analysis. Besides, Fe_3O_4@F127@FA nanoclusters showed good compatibility in the tested concentration range and good sensitivity in T_2-weighted MRI. The magnetic nanoclusters combined with drug delivery properties have greatly increased the significance in the diagnosis and therapy of diseases, which are suitable for systematical administration of hydrophobic drugs and simultaneously MRI diagnosis.

Introduction

Magnetic nanoparticles have gained great attention in biomedical areas, such as drug targeted delivery and MRI imaging.[1–3] Among magnetic nanoparticles, superparamagnetic Fe_3O_4 nanoparticles are especially amazing for their good biocompatibility and magnetic targeted ability. Some products based on superparamagnetic Fe_3O_4 nanoparticles has already been approved in clinical trials.[4] Among many synthetic methods, high-temperature thermolysis has been favorable for producing Fe_3O_4 nanoparticles with narrow size distribution and good crystallinity.[5] However, this approach usually produces nanoparticles with hydrophobic surfaces, which greatly limits their application in the bio-medicine field. To solve this problem, varieties of methods have been developed to improve the water solubility, such as ligand exchange.[6,7] For drug delivery, magnetic nanoparticles are generally modified with mesoporous silica or polymers, and the drugs are usually chemically conjugated or physically adsorbed.[8–10] These processes are complex and usually involve multiple steps. Besides, this formulation also brings low iron content and therefore results in the decrease in magnetic targeting ability. Since folate receptor is over expressed in many human tumors, folic acid (FA, $C_{19}H_{19}N_7O$) can be a good potential targeting ligand due to its high-affinity for the folate receptor.[11] It has been reported that FA conjugated nanostructures are endocytosed following a receptor-mediated way by binding to FA receptors, therefore can deliver therapeutics of interest to tumor cells.[12] Previous studies have showed that folic acid modified nanostructures had excellent targeting ability to tumor cells.[13,14]

Here we prepared Fe_3O_4@F127 nanoclusters using the hydrophobic Fe_3O_4 nanoparticles and Pluronic copolymer poly(ethylene oxide)–poly(propylene oxide)–poly(ethylene oxide) (PEO_{100}–PPO_{65}–PEO_{100}, F127) as starting materials by a one-step ultrasonic method. F127 was selected because it is a kind of biocompatible copolymer, whose hydrophobic segment can encapsulate drugs or fluorophores and hydrophilic segment can provide the water-soluble properties.[15–17] Compared with dextran or other polymer, the drug can be loaded by physical encapsulation because of its self-assemble behavior while using F127 coated Fe_3O_4 nanoparticles. Some similar system has been

[a]*The First Affiliated Hospital, Anhui Medical University, 218 Jixi Road, Hefei, Anhui, PR China. E-mail: ayfyyuyongqiang@126.com; Tel: +86-551-62922381*

[b]*School of Basic Medical Sciences, Anhui Medical University, 81 Meishan Road, Hefei, Anhui, PR China. E-mail: shenyx@ahmu.edu.cn; Tel: +86-551-65113776*

[c]*Biopharmaceutical Institute, Anhui Medical University, 81 Meishan Road, 230032 Hefei, China*

[d]*School of Pharmacy, Anhui Medical University, 81 Meishan Road, Hefei, Anhui, PR China*

† Electronic supplementary information (ESI) available. See DOI: 10.1039/c9ra09670a

‡ These authors contributed equally to this work.

reported for drug delivery and MR diagnosis. For instance, Lin *et al.*[18] reported a magnetic nanocarrier modified by FA and F127 as MR imaging contrast agents and drug carriers. This system first prepared F127–FA adduct and then chemically conjugated to poly(acrylic acid) (PAA)-coated Fe_3O_4 nanoparticles. Compared with the previous work, our study has merits. First, the initial Fe_3O_4 nanoparticles are hydrophobic and the small size makes them easily excreted by kidney, which was not beneficial for application *in vivo*. After a simple treatment, the products are water-soluble, polyethylene glycol modified and have appropriate diameters. The surface polymer coating plays important roles in prolonging the circulation time and the terminal hydroxyl groups can be used to further conjugation. Additionally, each nanocluster contains large amounts of Fe_3O_4 nanoparticles instead of one particle, which improved the magnetic properties and therefore was beneficial for MR imaging and magnetic targeting. Last but not least, this formulation makes the drug loading simultaneously without multiple steps and therefore protects its pharmacological activity.

In this study, FA targeted magnetic nanoclusters (Fe_3O_4@F127@FA) were prepared by a facile ultrasonic-treated and the drugs can be also loaded simultaneously. The morphology, size and magnetic properties of synthesized nanoclusters were analyzed. The drug targeted delivery performance of the nanoclusters was also investigated at cell level by measure the internalized cellular iron mount and cell viability.

Materials and methods

Materials

Pluronic F127 and 3-[4,5-dimethylthiazol-2-yl]-2,5-diphenyl tetrazolium bromide (MTT) were purchased from Sigma-Aldrich. Oleic acid, oleylamine, benzyl alcohol and folic acid were acquired from Sinopharm Chemical Reagent Co., Ltd. HepG2 (liver hepatocellular carcinoma) cells were acquired from the Type Culture Collection of the Chinese Academy of Sciences, Shanghai, China.

Synthesis of Pluronic F127–FA conjugates

As shown in Fig. S1,† the conjugation of Pluronic F127 to FA was synthesized using a similar method according to the previous published literature.[18] Briefly, 0.483 g of FA was dissolved in dimethylsulfoxide (DMSO, 15 mL) and then *N*,*N*′-carbonyldiimidazole (CDI, 0.176 g) was added. The mixture was stirred overnight at room temperature in the dark. F127 (3.1 g) was added to the above mixture and stirred for another 24 h. Then, the reaction solution was dialyzed for three days with deionized water, which was required to change deionized water every 3–6 h. Finally, the product was lyophilized for further use.

Synthesis of Fe_3O_4@F127, Fe_3O_4@F127@FA nanoclusters

The hydrophobic OA-coated Fe_3O_4 were prepared as the previous publication.[19] The hydrophobic Fe_3O_4 nanoparticles was dissolved in cyclohexane (10 mL) and F127 (50 mg) or Pluronic F127–FA was dissolved in deionized water (20 mL). Subsequently, the above two solutions were mixed and ultrasonic-treated sufficiently. Then the resulting solution was centrifuged (12 000 rpm, 10 min) and dissolved in deionized water.

Characterizations

The morphology of nanoclusters was observed by transmission electron microscope (TEM, JEM-2010, JEOL, Tokyo, Japan). The particle size of nanoclusters was measured by dynamic light scattering (DLS, NanoZS90, Malvern Instruments Ltd., UK). The crystal structure of nanoclusters was characterized by using X-ray diffraction (XRD, DMAX 2000, Rigaku, Japan). MR relaxivity of OA-coated Fe_3O_4 nanoparticles, Fe_3O_4@F127 and Fe_3O_4@F127@FA nanoclusters were measured by an MR scanner at 3.0 T (GE, Milwaukee, USA). T_2 imaging was carried as follows: echo time (TE) = 20, 40, 60, 80, 100 and 120 ms; repetition time (TR) = 3000 ms; field of view (FOV) = 20 mm × 20 mm; slice thickness = 4.0 mm; matrix = 320 × 320.

Drug loading and release

For doxorubicin (DOX) loading, appropriate amount of DOX was added into the mixture of hydrophobic Fe_3O_4 nanoparticles, Pluronic F127 (50 mg) or Pluronic F127–FA. Subsequently, the above two solution were mixed together and ultrasonic-treated sufficiently. Then the resulting solution was centrifuged (12 000 rpm, 10 min) and dissolved in deionized water (2 mL). The method how to determine DOX loading was referred according to the previous publication.[20] The resulting solution (400 μL) was centrifuged (12 000 rpm, 10 min), then the precipitate was lyophilized for two days. 12.5% v/v methanol in chloroform solution (2 mL) was added in the lyophilized sample to extract DOX. The sample solution was shook on shaker rotating at room temperature for 24 h, and then centrifuged (12 000 rpm, 10 min). Subsequently, the concentration of DOX in the supernatant was measured to determine the drug loading content. DOX-loaded nanoclusters were immersed in release media at pH = 5.0 and pH = 7.4, respectively. The concentration of DOX in buffer was measured at the given time points and then the cumulative release amount was calculated.

In vitro toxicity studies

3-[4,5-dimethylthiazol-2-yl]-2,5-diphenyl tetrazolium bromide (MTT) assay. HepG2 cells were pre-grown in 96-well plates with a density of 1×10^4 cells per well for 24 h. Then the cells were incubated with Fe_3O_4@F127, Fe_3O_4@F127@FA, Fe_3O_4@F127@DOX, Fe_3O_4@F127@FA@DOX. The detailed process of MTT assay was referred to the previous literature.[21]

Cell apoptosis. HepG2 cells were seeded in 6-well culture plates at a density of 5×10^5 cells. After 24 h, the cells were incubated with Fe_3O_4@F127, Fe_3O_4@F127@FA, Fe_3O_4@F127@DOX, Fe_3O_4@F127@FA@DOX and DOX. Then the cell apoptosis was measured by the protocol of the manufacture. At the completion of incubation, cells were collected and stained by Annexin V-FITC (5 μL) and propidium iodide (PI, 10 μL) and then measured by using a flow cytometer (FACSCalibur, BD, USA).

Cellular uptake studies

Laser scanning confocal microscopy (CLSM). The HepG2 cells were seeded in 24-well culture plates with a density of 5×10^4 cells. The cells were incubated with Fe_3O_4@F127@DOX, Fe_3O_4@F127@FA@DOX, Dulbecco's modified Eagle's medium (DMEM) and DOX overnight. After that, these cells were fixed and then the cell actin and nucleus were stained with fluorescent dyes. Finally the cells were photographed with laser scanning confocal microscope (LSM800, Zeiss, German).

Inductively coupled plasma (ICP) analysis. The HepG2 cells were seeded into a 24-well plate at a density of 5×10^4 cells per well. The cells were incubated with Fe_3O_4@F127 nanoclusters or Fe_3O_4@F127@FA nanoclusters at the same iron concentration. After 24 h, the cells were collected, and then the intracellular Fe concentration was measured by ICP (Agilent 730 ICP-OES, USA).

***In vitro* MRI.** T_2-weighted signal intensities were calculated with a 3.0 T MR scanner using iron concentration ranging from 0 to 40 μM. For cell MRI, these cell samples were collected and then dispersed in 0.1% agarose gel. T_2 imaging was acquired as follows: TR = 3000 ms, TE = 100 ms, FOV = 60 mm × 48 mm, slice thickness = 4.0 mm.

Results

Materials characterization of Fe_3O_4@F127 nanoclusters

FA targeted magnetic nanoclusters (Fe_3O_4@F127@FA) were prepared by a facile ultrasonic-treated. As shown in Scheme 1, FA, hydrophobic Fe_3O_4 nanoparticles, and F127–FA aqueous solution were mixed. After sufficient ultrasonic treatment, Fe_3O_4 nanoparticles were transferred to aqueous phase and encapsulated with F127 and FA. Besides, DOX were used as modeling drug molecules and added to the initial system to obtain drug-loaded nanoclusters (Fe_3O_4@F127@FA@DOX).

TEM characterization was performed to study the morphology (Fig. 1a). After ultrasonic treatment, a lot of nanoclusters were seen under TEM observation. As shown in Fig. 1b, each aggregate was consisted of many small Fe_3O_4 nanoparticles, and therefore we named it nanocluster. DLS results showed that the dynamic diameter distributed from 250 to 350 nm (Fig. 1c), which are larger than the size from TEM observation, suggesting the surface polymer are stretched in the aqueous solution. Fig. 1d shows the typical digital photos before and after the formation of Fe_3O_4@F127 nanoclusters. After the ultrasonic treatment, the black product was transferred from the upper organic phase to the lower aqueous phase, which suggests it is successful in formation of Fe_3O_4@F127 nanoclusters. The crystal structure of Fe_3O_4@F127 nanoclusters was confirmed by XRD. As shown in Fig. S2,† the XRD pattern reveals the formation of single-phase inverse spinel magnetite (JCPDS card no. 88-0315).

FA, a widely used targeting ligand for tumors, was selected to modify Fe_3O_4@F127 nanoclusters to enhance the cellular uptake. In order to prove the conjugation of FA to F127, IR characterization was carried. Fig. 1e clearly shows a characteristic peak located 1340 cm^{-1} in the spectrum of Fe_3O_4@F127@FA, which is ascribed to the newly formed ester bond of F127 and FA. The peak of Fe–O was seen at 580 cm^{-1}. The peaks appeared at 3420 and 3300 cm^{-1} are ascribed to amine bond of FA. The broad peak between 1200 and 1000 cm^{-1} is ascribed to the C–O stretching vibration of the Pluronic copolymer. The peak of C–H was found at 2920, 2850 and 1380 cm^{-1}. The presence of most of these characteristic functional groups of FA in Fourier transform infrared (FTIR) spectrum of Fe_3O_4@F127@FA confirmed its conjugation to Fe_3O_4@F127. Additionally, a UV-vis spectrum was also carried to see whether FA was modified successfully. As expected, Fe_3O_4@F127@FA showed a UV peak in the range of 210 to 400 nm, which is similar to that of FA.

MRI properties

For magnetic nanoparticles, it is important that nanomaterials keep their magnetic properties after modification or decoration for biological applications as MRI contrast agents. The MRI

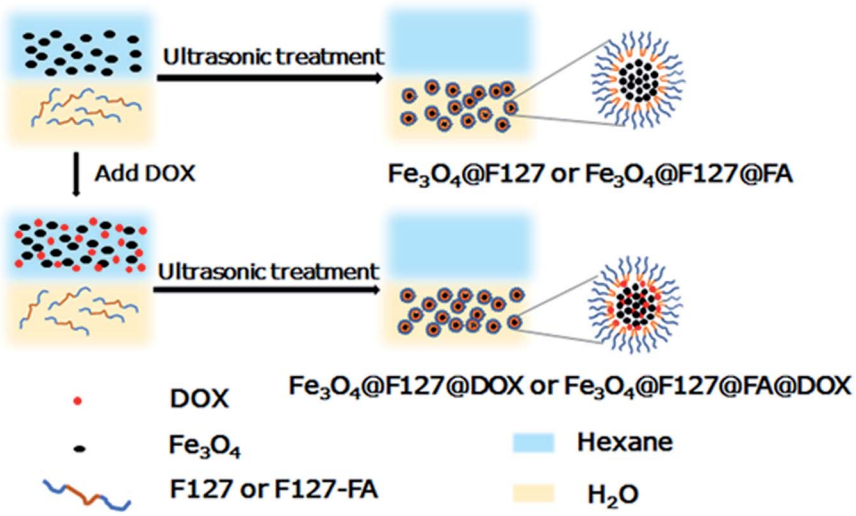

Scheme 1 Schematic representing the formulation of Fe_3O_4@F127@FA and the drug loading process.

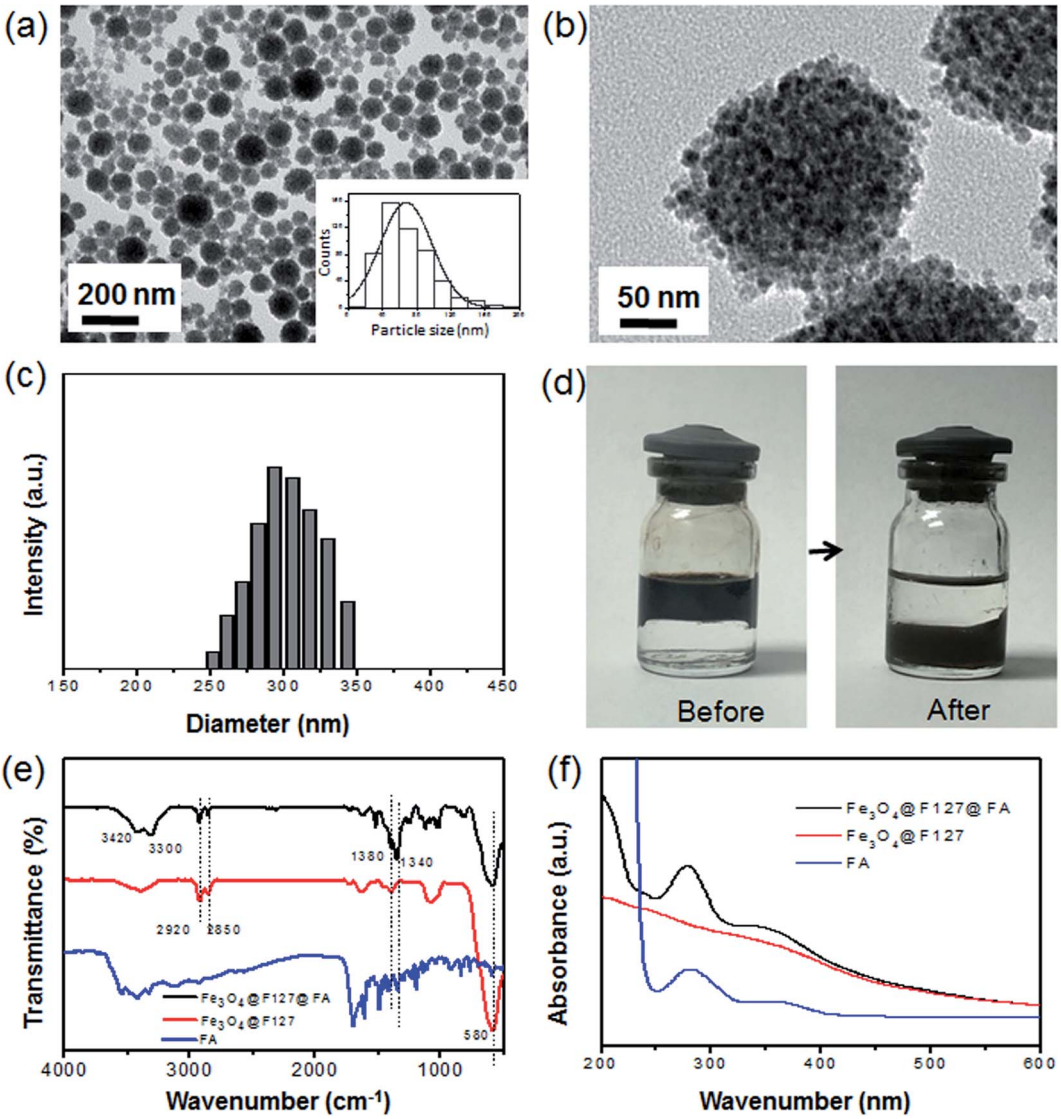

Fig. 1 Characterizations of Fe_3O_4@F127 nanoclusters. (a and b) TEM characterization of Fe_3O_4@F127@FA nanoclusters. (c) Size distribution of Fe_3O_4@F127@FA nanoclusters. (d) Digital photos of before and after the formation of Fe_3O_4@F127 nanoclusters. (e) IR spectra of FA, Fe_3O_4@F127 nanoclusters and Fe_3O_4@F127@FA nanoclusters. (f) UV-vis spectra of FA, Fe_3O_4@F127 nanoclusters, and Fe_3O_4@F127@FA nanoclusters.

properties of OA–Fe_3O_4 nanoparticles, Fe_3O_4@F127 nanoclusters, and Fe_3O_4@F127@FA nanoclusters were evaluated by calculating T_2 transverse relaxation time. The transverse relaxivity (r_2) value of single OA–Fe_3O_4 nanoparticles obtained by linear fit of $1/T_2$ and the concentration was 207.9 mM^{-1} s^{-1}. Similarly, r_2 values of Fe_3O_4@F127 nanoclusters and Fe_3O_4@F127@FA nanoclusters were about 406.13 mM^{-1} s^{-1} and 401.83 mM^{-1} s^{-1}, respectively. It was also found that T_2 signal was changed in a concentration-dependent manner (Fig. 2).

Drug loading and release

Since Fe_3O_4@F127@FA@DOX nanoclusters have the feasibility for drug delivery, their drug loading capacity was evaluated using DOX as a modelling drug due to its wide application in anti-cancer chemotherapy. Drug loading were carried simultaneously during the preparation process. The loading of DOX can be reflected from the color change of the supernatant aqueous liquid after ultrasonic treatment. After drug loaded, we calculated the encapsulation efficiency of doxorubicin is 70.36%, and the drug loading content is 14.07 wt%. To investigate the drug release behavior of Fe_3O_4@F127@DOX and Fe_3O_4@F127@FA@DOX nanoclusters, the drug release experiment was performed in buffer (pH = 7.4 and pH = 5.0) at 37 °C. The release of DOX can be judged directly from the color of sink medium. As shown in Fig. S3,† DOX-loaded Fe_3O_4@F127 nanoclusters exhibited a slow release in neutral environment and approximately 10% of the drug was released at the early period, then a more stable release of the smaller dosage was observed in the following 60 h. In contrast, DOX release rate was evidently increased at pH = 5.0. More than 10% of DOX released around 1 h, and the release reached a plateau within 12 h and over 30% of DOX was released.

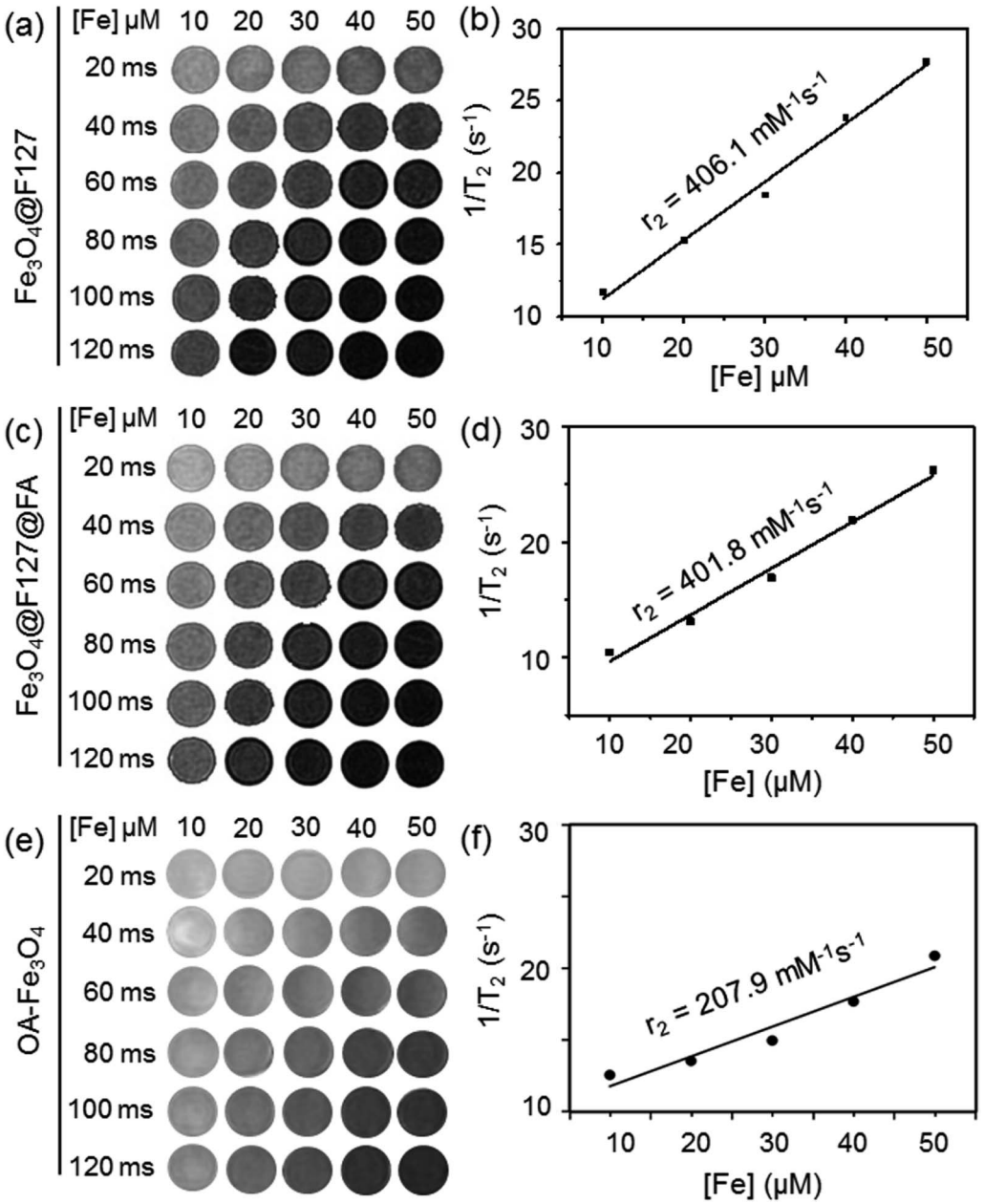

Fig. 2 MR properties of OA–Fe_3O_4 nanoparticles, Fe_3O_4@F127 nanoclusters, and Fe_3O_4@F127@FA nanoclusters. (a, c and e) T_2 images of OA–Fe_3O_4 nanoparticles, Fe_3O_4@F127 nanoclusters, and Fe_3O_4@F127@FA nanoclusters under different TE time. (b, d and f) T_2 relaxivity plot of OA–Fe_3O_4 nanoparticles, Fe_3O_4@F127 nanoclusters, and Fe_3O_4@F127@FA nanoclusters *versus* iron concentration.

In vitro MR studies

MRI was used to evaluate the potential of Fe_3O_4@F127@FA nanoclusters as MR contrast agents for tumor cells. HepG2 cells were incubated with Fe_3O_4@F127@FA nanoclusters for 24 h, Fe_3O_4@F127 nanoclusters were used as control. The color of MRI images becomes dark along with the increase of nanoclusters concentration, suggesting the increase of cellular uptake of magnetic nanoparticles. The cells incubated with DMEM were used as reference with MR intensity at 100%. The average signal intensity plotted against Fe concentrations are shown in Fig. 3c and d, which also showed the cellular uptake of Fe_3O_4@F127 nanoclusters and Fe_3O_4@F127@FA nanoclusters were concentration-dependent.

Toxicity studies

The cytotoxicity of Fe_3O_4@F127 nanoclusters or Fe_3O_4@F127@FA nanoclusters were conducted by using MTT assay and the bar chart was depicted in Fig. 4a. It was found that the viability of the cells exposed the two materials has no significant difference compared with control cells. In order to quantitatively assess the cytotoxicity of Fe_3O_4@F127 nanoclusters and Fe_3O_4@F127@FA nanoclusters, flow cytometry was also used.

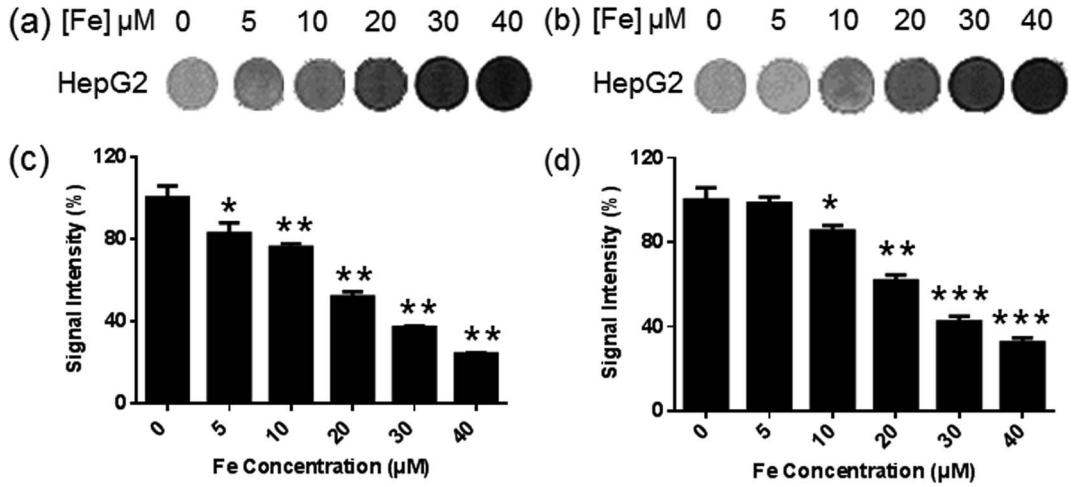

Fig. 3 T_2-weighted MR images of HepG2 cells incubated with Fe_3O_4@F127 nanoclusters (a) and Fe_3O_4@F127@FA nanoclusters (b) *in vitro*. The average signal intensity of Fe_3O_4@F127 nanoclusters (c) and Fe_3O_4@F127@FA nanoclusters (d) plotted against Fe concentrations.

As is shown in the Fig. 4b–d, when HepG2 cells were incubated with Fe_3O_4@F127 nanoclusters and Fe_3O_4@F127@FA nanoclusters at a concentration of 40 μM, the apoptotic rate of HepG2 cells was only 2.98% and 3.037%, which has no significant difference compared with control cells incubated with DMEM. The results further demonstrate that these carriers have good biocompatibility in the tested concentration range.

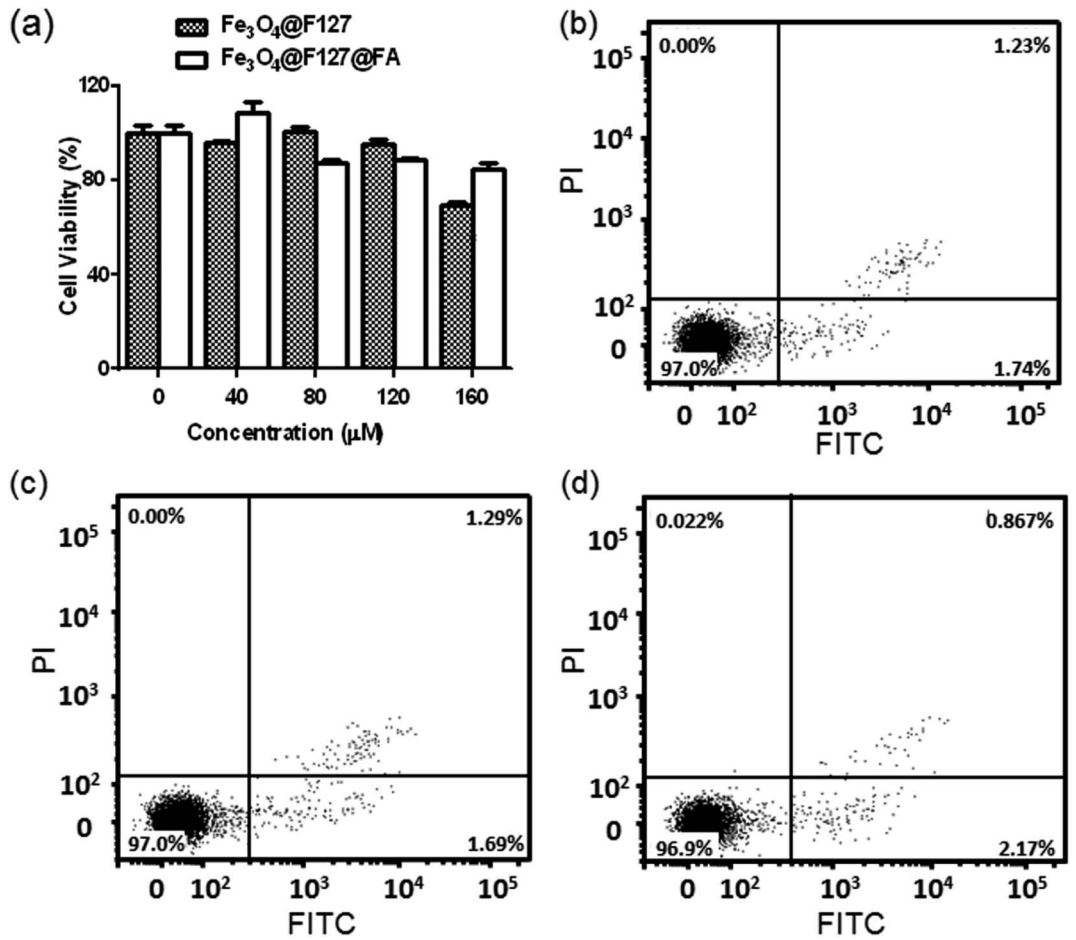

Fig. 4 *In vitro* toxicity studies. (a) Cell viability of HepG2 cells exposed to Fe_3O_4@F127 nanoclusters and Fe_3O_4@F127@FA nanoclusters. (b–d) Apoptotic HepG2 cells were detected by flow cytometry after exposed to DMEM (b), Fe_3O_4@F127 nanoclusters (c), and Fe_3O_4@F127@FA nanoclusters (d) with iron concentration of 40 μM.

Targeted drug delivery

Since DOX exhibits brilliant red fluorescence, HepG2 cells incubated with DOX-loaded Fe_3O_4@F127 nanoclusters and DOX-loaded Fe_3O_4@F127@FA nanoclusters for 4 h are imaged under CLSM observation (Fig. 5). In order to determine the cellular localization of the nano materials, actin was also labeled by using FITC. We found the red fluorescence mainly classified into two types. One is located in the cytoplasm as a brilliant red pot, which is derived from DOX-loaded nanoclusters, other is in nuclei. When DOX-loaded nanoclusters were directly co-incubated with HepG2 cells, the nuclei are found to be stained in red fluorescence. We thought the red fluorescence in nucleus in DOX-loaded nanoclusters group may come from DOX released from the internalized DOX-loaded nanoclusters under cellular acidic environment. DOX-loaded Fe_3O_4@F127@FA nanoclusters show stronger fluorescent intensities compared with DOX-loaded Fe_3O_4@F127 nanoclusters.

The cellular iron content was calculated by using ICP to quantify the cellular uptake of nanoclusters. Intracellular Fe concentration of Fe_3O_4@F127@FA nanoclusters was higher than that of the Fe_3O_4@F127 nanoclusters (Fig. 6a). Moreover, as the sample concentration increases, the concentration of intracellular Fe^{3+} also increases. This result is in accordance with MTT results. After HepG2 cells were incubated with DOX-loaded Fe_3O_4@F127 nanoclusters and DOX-loaded Fe_3O_4@F127@FA nanoclusters, the cell viability was detected by MTT. As shown in Fig. 6b, DOX-loaded Fe_3O_4@F127 nanoclusters and DOX-loaded Fe_3O_4@F127@FA nanoclusters in solution exhibited the typical concentration-dependent antiproliferative effect in HepG2 cells. DOX-loaded Fe_3O_4@F127@FA nanoclusters showed a higher toxicity to the cells, which may be related to the enhanced uptake of the drug delivery system with the aid of FA.

Flow cytometry was also used to quantify the cell apoptosis rate of HepG2 cells after incubated with Fe_3O_4@F127@DOX nanoclusters and Fe_3O_4@F127@FA@DOX nanoclusters. As shown in Fig. 6c and d, treated with the same DOX

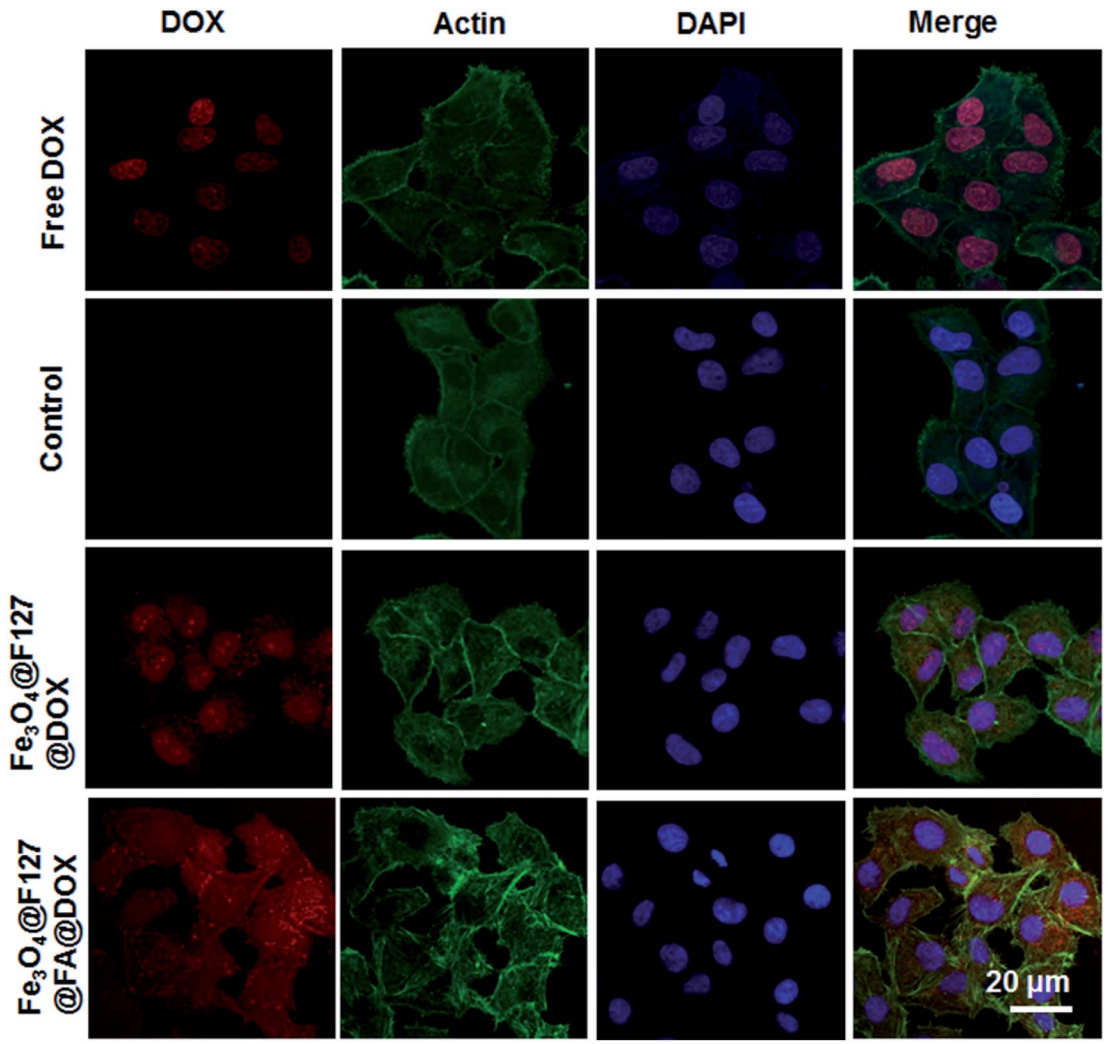

Fig. 5 Images of Fe_3O_4@F127@DOX and Fe_3O_4@F127@FA@DOX nanoclusters at a DOX concentration of 10 μM in HepG2 cells after co-incubation for 4 h taken under confocal microscopy. Blue, cell nuclei; red, DOX fluorescence; green, actin. Scale bar: 20 μm.

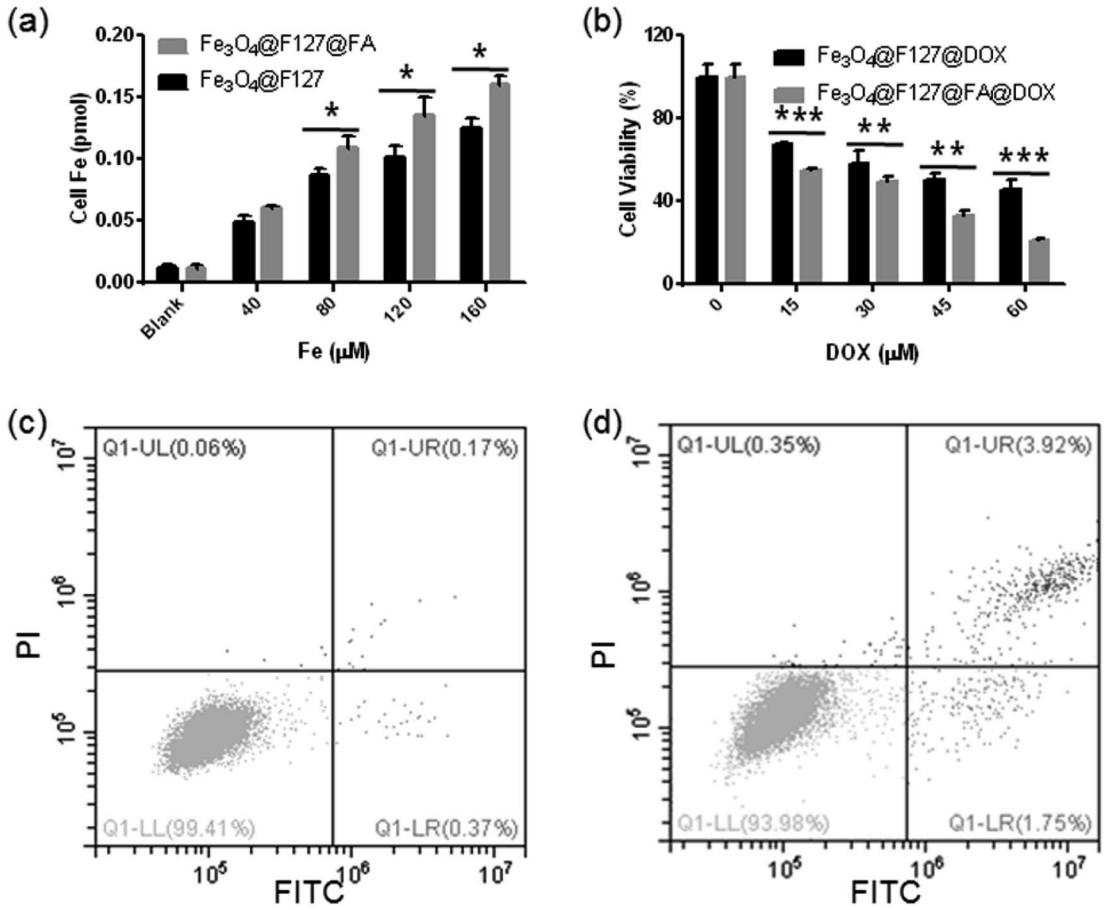

Fig. 6 (a) Cellular iron amount of HepG2 cells incubated with Fe_3O_4@F127 nanoclusters and Fe_3O_4@F127@FA nanoclusters. (b) Cell viability of HepG2 cells incubated with Fe_3O_4@F127@DOX nanoclusters and Fe_3O_4@F127@FA@DOX nanoclusters for 24 h. (c and d) Target ability evaluation of Fe_3O_4@F127@FA nanoclusters. Apoptotic HepG2 cells were detected by flow cytometer after incubation with Fe_3O_4@F127@DOX nanoclusters (c) and Fe_3O_4@F127@FA@DOX nanoclusters (d) with DOX concentration of 10 μM.

concentration, Fe_3O_4@F127@FA@DOX nanoclusters exposure leads to a higher apoptosis rate of HepG2 cells than that with Fe_3O_4@F127@DOX nanoclusters, which also indicates the targeting ability of FA.

Discussion

Oleic acid, magnetic nanoparticles, Pluronic polymers and folic acid are usual water dispersible nanoparticle-based formulation to increase the water dispersibility, targeting ability and biosafety. Recently, Hieu *et al.*[22] reported a similar system for cancer diagnosis. First, magnetic Fe_3O_4 nanoparticles were prepared by the co-precipitation method and then stabilized by F127–FA. Our study describes a simple way to prepared multifunctional nanoclusters for both MR imaging and drug targeted drug delivery. Oleic acid modified Fe_3O_4 nanoparticles are synthesized by a solvent thermal method, which can only dispersible in nonpolar solvents such as hexane and chloroform. After facile ultrasonic treatment, OA is covered by Pluronic layers and hydrophilic nanoclusters are formed by large amounts of single hydrophobic nanoparticles, which transfer Fe_3O_4 nanoparticles from hydrophobic organic phase to hydrophilic phase, this process can be clearly reflected by the digital photos of Fig. 1d. F127 coating is a critical step for the drug delivery application of nanomaterials, which can prevent the rapid clearance by RES (reticuloendothelial system) and prolong the circulation.[23] Therefore, Fe_3O_4@F127 nanoclusters can show good performance in drug delivery for systemic administration of a variety of hydrophobic agents.

IR data further shows the successful coating of F127. As shown in IR spectra, folic acid is chemically conjugated to F127 rather adsorbed onto the nanoparticles. Besides, the characteristic absorption peak of FA at 280 nm was also shown in the UV spectrum of Fe_3O_4@F127@FA nanoclusters solution.

For T_2 MRI agents, r_2 is an important parameter. For single nanoparticle, the r_2 value of Fe_3O_4 nanoparticles is 207.9 mM^{-1} s^{-1} which is smaller than that of the nanoclusters. The r_2 value of Fe-based aggregates or clusters with different coating materials published ranged from 100 mM^{-1} s^{-1} to 900 mM^{-1} s^{-1}.[24] For instance, Paquet *et al.* assembled 9.1 ± 2.1 nm Fe_3O_4 nanoparticles within a hydrogel coating and the product showed a high r_2 value of 505 mM^{-1} s^{-1} at 3.0 T.[25] Li *et al.* observed a r_2 value of PEI (polyetherimide)-decorated Fe_3O_4 nanoparticles as high as 475.92 mM^{-1} s^{-1} at 3.0 T.[26] The r_2 value

of Fe_3O_4@F127 nanoclusters and Fe_3O_4@F127@FA nanoclusters are 406.13 mM^{-1} s^{-1} and 401.83 mM^{-1} s^{-1} under 3.0 T. The results indicated that the formulation components F127 and FA modification have no significant influence on the MRI properties of the core Fe_3O_4 nanoparticles. As commercial T_2 contrast agents, the r_2 value of Feridex is 108.2 mM^{-1} s^{-1}, it is believed that our formulation would be a kind of effective T_2 contrast agent.

Efficient drug loading and controlled release are necessary for drug delivery system. Following our method, drugs are distributed in the oleic acid shell of Fe_3O_4 nanoparticles without chemical conjugation, which is very simple and keep the activity of the drugs. Drug loading is the result of the interaction of the hydrophobic cavity with the hydrophobic drug, therefore the delivery system can be loaded by other hydrophobic drugs. Previous literature showed that magnetic particles coated with starch with phosphate shown the amount of drug is 0.8 wt%.[27] Jain *et al.* reported a similar OA–Pluronic Fe_3O_4 nanoformulation with a drug loading amount of 8.2 wt%. Nasongkla *et al.* reported multifunctional nanocomposites with drug delivery and MR imaging characteristics with the loading efficiency of DOX is 2.7 wt%.[28] The amount of DOX loading of our Fe_3O_4@F127@FA formulation is optimal (14.72 wt%), which demonstrated Fe_3O_4@F127@FA nanoclusters would be good vehicles for drug delivery. DOX loaded in both Fe_3O_4@F127@FA@DOX nanoclusters and Fe_3O_4@F127@DOX nanoclusters displayed sustained release behavior over 60 h. FA modification has weak significance on the release behavior. However, only 10% DOX was released at pH = 7.4 within 60 h. The difference of release profiles may be ascribed to that surface hydrophilic PEO (polyethylene oxide) chains became more stretched under acidic environment.[29] This result implied that the release of drug from Fe_3O_4@F127 nanoclusters could be very slow during blood circulation in normal tissue, while the release rate is accelerated in tumor tissue. Therefore, drugs can be effectively delivered to tumor sites which can reduce side effects. Besides, good compatibility is of chief importance for drug delivery. Both MTT and FACS results showed the targeted delivery carrier had low cytotoxicity in the tested concentrations.

The targeting role of FA can be reflected through toxicity results of both FA-conjugated and unconjugated nanoclusters, CLSM results and ICP results. First, ICP analysis manifested that cellular iron content of Fe_3O_4@F127@FA nanoclusters group higher than unconjugated Fe_3O_4@F127 nanoclusters group. CLSM observation indicated that cells incubated with FA-conjugated nanoclusters displayed stronger fluorescence in comparison with unconjugated nanoclusters. MTT results also showed that cells incubated with FA-conjugated DOX loaded nanoclusters have lower viability than unmodified DOX loaded nanoclusters. All these results demonstrated that folic acid plays an active targeting role of in the process of cellular uptake.

Conclusion

This paper reported a facile ultrasonic-treated method to prepare water-soluble Fe_3O_4@F127@FA nanoclusters. The nanoclusters have an r_2 value as high as 401.83 mM^{-1} s^{-1} under 3.0 T and good biocompatibility. Besides, DOX can also be loaded during the ultrasonic treatment to form the nano drug delivery system, which showed good drug loading effect and controlled release behavior. CLSM study and cellular uptake Fe content analysis indicated that FA conjugated drug delivery system enhanced the cellular uptake and therefore showed higher cytotoxicity. It is anticipated that the formulations combined of targeting drug delivery and MRI agents could be employed for therapeutics of cancer.

Conflicts of interest

The authors declare no conflict of interest.

Acknowledgements

This work was supported by the National Natural Science Foundation of China (Grant No. 51302004 to Meng-Meng Song), Scientific Research Foundation of the Institute for Translational Medicine of Anhui Province (SRFITMAP, 2017zhyx34) and Anhui Provincial Natural Science Foundation of China (Grant No. 1308085QH141 to Meng-Meng Song).

References

1 C. Sun, J. S. H. Lee and M. Q. Zhang, *Adv. Drug Delivery Rev.*, 2008, **60**, 1252–1265.
2 R. Tietze, J. Zaloga, H. Unterweger, S. Lyer, R. P. Friedrich, C. Janko, M. Pottler, S. Dürr and C. Alexiou, *Biochem. Biophys. Res. Commun.*, 2015, **468**, 463–470.
3 T. Y. Liu, S. H. Hu, K. H. Liu, R. S. Shaiu, D. M. Liu and S. Y. Chen, *Langmuir*, 2008, **24**, 13306–13311.
4 R. R. Jin, B. B. Lin, D. Y. Li and H. Ai, *Curr. Opin. Pharmacol.*, 2014, **18**, 18–27.
5 L. H. Reddy, J. L. Arias, J. Nicolas and P. Couvreur, *Chem. Rev.*, 2012, **112**, 5818–5878.
6 J. Xie, C. Xu, N. Kohler, Y. Hou and S. Sun, *Adv. Mater.*, 2007, **19**, 3163–3166.
7 T. R. Zhang, J. P. Ge, Y. X. Hu and Y. D. Yin, *Nano Lett.*, 2007, **7**, 3203–3207.
8 W. L. Cai, M. Y. Guo, X. L. Weng, W. Zhang and Z. L. Chen, *Mater. Sci. Eng., C*, 2019, **98**, 65–73.
9 Y. L. Liu, D. Chen, P. Shang and D. C. Yin, *J. Controlled Release*, 2019, **302**, 90–104.
10 E. Guisasola, M. Vallet-Regí and A. Baeza, in *Stimuli Responsive Polymeric Nanocarriers for Drug Delivery Applications*, ed. A. S. H. Makhlouf and N. Y. Abu-Thabit, Woodhead Publishing, Cambridge, 2018, vol. 1, pp. 143–168.
11 X. Zhao, H. Li and R. J. Lee, *Expert Opin. Drug Delivery*, 2008, **5**, 309–319.
12 P. Suriamoorthy, X. Zhang, G. Hao, A. G. Joly, S. Singh, M. Hossu, X. Sun and W. Chen, *Cancer Nanotechnol.*, 2010, **1**, 19–28.
13 Y. T. Liu, K. Li, J. Pan, B. Liu and S. S. Feng, *Biomaterials*, 2010, **31**, 330–338.

14 J. J. Xu, B. Xu, D. Shou, F. H. Qin and Y. Hu, *Eur. J. Pharm. Sci.*, 2016, **83**, 132–142.
15 S. Chen, Y. Li, C. Guo, J. Wang, J. H. Ma, X. F. Liang, L. R. Yang and H. Z. Liu, *Langmuir*, 2007, **23**, 12669–12676.
16 C. G. Hiremath, G. B. Heggnnavar, M. Y. Kariduraganavar and M. B. Hiremath, *Prog. Biomater.*, 2019, **8**(3), 155–168.
17 K. C. Barick, E. Ekta, S. L. Gawali, A. Sarkar, A. Kunwar, K. I. Priyadarsini and P. A. Hassan, *RSC Adv.*, 2016, **6**, 98674–98681.
18 J. J. Lin, J. S. Chen, S. J. Huang, J. H. Ko, Y. M. Wang, T. L. Chen and L. F. Wang, *Biomaterials*, 2009, **30**, 5114–5124.
19 F. Wang, X. L. Chen, Z. X. Zhao, S. Tang, X. Huang, C. Lin, C. Cai and N. Zheng, *J. Mater. Chem.*, 2011, **21**, 11244.
20 T. K. Jain, J. Richey, M. Strand, D. L. Leslie-Pelecky, C. A. Flask and V. Labhasetwar, *Biomaterials*, 2008, **29**, 4012–4021.
21 M. M. Song, H. L. Xu, J. X. Liang, H. H. Xiang, R. Liu and Y. X. Shen, *Mater. Sci. Eng., C*, 2017, **77**, 904–911.
22 H. V. Quang, M. S. Vinding, T. Nielsen, M. G. Ullisch, N. C. Nielsen, D. T. Nguyen and J. Kjems, *Polymers*, 2019, **11**, 743.
23 J. S. Tan, D. E. Butterfield, C. L. Voycheck, K. D. Caldwell and J. T. Li, *Biomaterials*, 1993, **14**, 823–833.
24 Z. W. Zhang, L. Liu, H. M. Chen, K. Hu, I. Delahunty, S. Gao and J. Xie, *Theranostics*, 2018, **8**, 2521–2548.
25 C. Paquet, H. W. Haan, D. M. Leek, H. Y. Lin, B. Xiang, G. H. Tian, A. Kell and B. Simard, *ACS Nano*, 2011, **5**, 3104–3112.
26 J. C. Li, Y. Hu, J. Yang, W. J. Sun, H. D. Cai, P. Wei, Y. P. Sun, G. X. Zhang, X. Y. Shi and M. W. Shen, *J. Mater. Chem. B*, 2015, **3**, 5720–5730.
27 C. Alexiou, W. Arnold and R. J. Klein, *Cancer Res.*, 2000, **60**, 6641–6648.
28 N. Nasongkla, E. Bey, J. Ren, H. Ai, C. Khemtong, J. S. Guthi, S. F. Chin, A. D. Sherry, D. A. Boothman and J. M. Gao, *Nano Lett.*, 2006, **6**, 2427–2430.
29 T. Fukuta, T. Ishii, T. Asai and N. Oku, *Biol. Pharm. Bull.*, 2019, **42**, 319–326.